We are IntechOpen,
the world's leading publisher of
Open Access books
Built by scientists, for scientists

6,900
Open access books available

186,000
International authors and editors

200M
Downloads

Our authors are among the

154
Countries delivered to

TOP 1%
most cited scientists

12.2%
Contributors from top 500 universities

CLARIVATE ANALYTICS
BOOK CITATION INDEX
INDEXED

WEB OF SCIENCE™

Selection of our books indexed in the Book Citation Index
in Web of Science™ Core Collection (BKCI)

Interested in publishing with us?
Contact book.department@intechopen.com

Numbers displayed above are based on latest data collected.
For more information visit www.intechopen.com

MHD Activity in an Extremely High-Beta Compact Toroid

Tomohiko Asai and Tsutomu Takahashi
Nihon University
Japan

1. Introduction

1.1 Field-reversed configuration (FRC)

A field-reversed configuration (FRC) plasma is extremely high beta confinement system and the only magnetic confinement system with almost 100% of a beta value (Tuszewski, 1988; Steinhauer, 2011). The plasma is confined by the only poloidal magnetic field generated by a self-plasma current. The FRC has several potentials for a fusion energy system. As the one of the candidate for an advanced fusion reactor, for example, D-3He fusion (Momota, 1992), FRC plasma is attractive. Recently, this plasma also has an attraction as target plasmas for an innovative fusion system, Magnetized Target Fusion (MTF) (Taccetti, 2003), Colliding and merging two high-β compact toroid (Guo, 2011; Binderbauer, 2010; Slough, 2007a) and Pulsed High Density FRC Experiments (PHD) (Slough, 2007b).

The plasma belongs to a compact toroid system. Here, 'compact' denotes a simply connected geometry, i.e., the absence of a central column. The system consists of a toroidal magnetic confinement system with little or no toroidal magnetic field. The typical magnetic structure of the FRC plasma is shown in Fig. 1. The poloidal confinement field (B_{ze}) consists of the externally applied magnetic field of an external coil (B_{z0}), and the self-generated magnetic field of the toroidal plasma current (I_θ : $I_\theta > 2B_{z0}/\mu_0$). The FRC consists of an axially symmetric magnetized plasma, a plasma liner and a simply connected configuration. Then, the beta value $\beta = p/\left(B_{ze}^2/2\mu_0\right)$), which is the ratio of confined plasma pressure (p) to the confinement magnetic field pressure ($B_{ze}^2/2\mu_0$), is extremely high. The system has a closed field line region in which the high temperature plasma is confined, and an open field line region which acts as a natural diverter.

A scrape-off layer is formed in the open field line region. Two singularities in the magnetic field, i.e., X-points, are formed at the intersections of the symmetric device axis with the separatrix ($B_{ze} = 0$). A null field surface ($B_z = 0$) is also formed in the closed separatrix region. The radius (R) of the null surface at midplane (minor radius) is $R = r_s/\sqrt{2}$ (r_s: radius of the separatrix at midplane) in the pressure equilibrium state. The separatrix length l_s is defined as the distance between the two X-points (Armstrong et al., 1981).

An FRC has three essential geometrical plasma parameters (S^*: radial size parameter; E: separatrix elongation; and X_s: normalized separatrix radius), which are related to the physical

properties of the FRC plasma. $S^* = r_s/(c/\omega_{pi})$ is defined as the ratio of the separatrix radius to the ion skin depth (c/ω_{pi}). Here, r_s, c and ω_{pi} are the separatrix radius, speed of light and ion plasma frequency, respectively. Two other radial size parameters, $S \equiv r_s/\sqrt{2}\rho_i$ and $\bar{s} = \int_R^{r_s} r \, dr/r_s\rho_i$, are sometimes used, where ρ_i and ρ_{io} are the local ion Larmor-radius and the reference ion Larmor-radius, respectively, based on the external magnetic field B_{ze}. These parameters indicate the importance of the two-fluid (ion and electron fluid) and finite-Larmor-radius effects; for example, $S \approx 1.3S^*$ and $\bar{s} = X_sS/5$ under under $T_i \sim 2T_e$ (T_i: ion temperature; T_e: electron temperature) (Steinhauer, 2011). $E = l_s/2r_s$ is defined as the ratio of the separatrix radius to the diameter, and indicates the elongation of the separatrix, which is different from that of a tokamak system. It is known that this elongation affects the global plasma stability of an FRC. Oblate and prolate FRC plasmas are usually categorized as $0 < E < 1$ and $E > 1$ FRCs, respectively. $X_s = r_s/r_w$ is defined as the ratio of the separatrix to the confinement coil radius. This normalized radius has a strong relation to the poloidal flux (ϕ_p) of an elongated (prolate) FRC plasma, and to the FRC confinement time scaling. The average beta value $\langle\beta\rangle$ can be written as $\langle\beta\rangle = 1 - 0.5x_s^2$ (Armstrong et al., 1981).
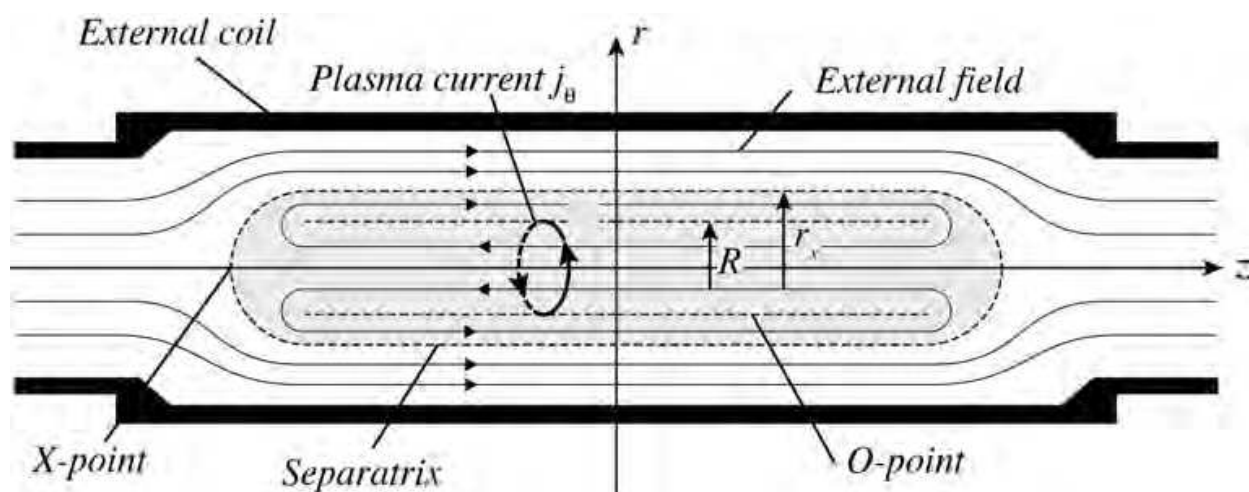

Fig. 1. A field-reversed configuration plasma formed by the field-reversed theta-pinch (FRTP) method.

The FRC topology is similar to an elongated, low-aspect-ratio, toroidal version of the Z-pinch, as shown in Fig. 1. Since the FRC plasma has no toroidal field, and no center conductor, theoretical studies predict that FRC plasma is unstable with respect to an MHD mode with low toroidal mode number. The principal instabilities of the FRC, predicted by magnetohydrodynamics (MHD) theory, are listed in Table 1 (Tuszewski, 1988; Slough & Hoffman, 1993). Here, the tokomak nomenclature has been adopted, with n and m being the toroial and poloidal mode numbers, respectively.

The plasma current of FRC, at just after formation, is primarily carried by electrons. On the other hand, ions are approximately at rest. However, in most of the FRC experiments, ions soon begin to rotate to a diamagnetic direction. The rotation speed often reaches to a supersonic level. Instabilities driven by the Rotational mode is appeared. The origin of

rotation has not yet been completely understood. But, given rotation, the condition for instability has been fairly well understood. The stability threshold was expressed in terms of a parameter $\alpha = \Omega / \Omega_{Di}$, where Ω and Ω_{Di} are rotation angular frequency and ion diamagnetic drift frequency. The threshold for n=1 mode was $\alpha=1$ and in n=2 mode could also grow for α greater than 1.2 -1.4, for zero bias limit (Freidberg & Pearlstein, 1978). For FRC plasma, a similar threshold is $\alpha \sim 1.3$-1.5 (Seyler, 1979).

	m (poloidal mode)	Mode Character	Mode Name	Experimental Observation
1. Local Ideal Mode				
∞	0		Interchange	Only lowest order (n=1,2,3)
∞	1,2	Axial or Radial	Co-interchange (Ballooning)	No
2. Global Mode				
No rotating				
0	1	Axial	Roman candle	No
1	0	Sausage Shift	Interchange	Often, occasional
1	1	Radial	Sideways shift (Tilt)	Seldom
>1	0	Flute	Interchange	Often, always (high-$\bar{s}$)
>1	1	Axial	Tilt	No
Rotating				
1	1	Radial	Wobble	Yes (occasional)
2	1	Radial	n=2	Yes (always)
>2	1	Radial	n>2	Yes (often, high-$\bar{s}$)
3. Resistive Mode				
0	2	Radial and Axial	Tearing	Yes (always?)

Table 1. FRC Stability: MHD Theory versus Experimental Observation

These two global ideal modes driven by rotation—the $n = 1$ wobble, of little concern since it saturates at low amplitude, and the $n = 2$ rotational instability, which destroys most FRCs—have been regularly observed experimentally. These rotational modes ($n = 1, 2$) have been controlled by applying a straight or helical multi-pole field (Ohi et al., 1983; Shimamura & Nogi, 1986; Fujimoto et al., 2002). Higher-order ($n > 2$) rotational modes have often been observed in large-$\bar{s}$ FRC experiments, with $\bar{s}$ in the region of $3 < \bar{s} < 8$ (Slough & Hoffman, 1993). FRC plasma with a higher $\bar{s}$ value behaves as a MHD plasma and with low $\bar{s}$ one becomes more kinematically. According to the several theoretical works, FRC plasmas have been predicted to be unstable because of a bad curvature of a closed confinement field. Various local and global non-rotating ideal MHD modes are listed in Table 1, and it is worth noting that stable FRC plasma is impregnable against these low n-modes. The m/n=1/1 tilt mode instability is thought to be most dangerous. The stability of prolate and oblate FRC plasma has been investigated experimentally on several FRTP

devices (FRX-C/LSM (Tuszewski et al., 1990, 1991), LSX, (Slough & Hoffman, 1993), NUCTE-III (Kumashiro et al., 1993; Asai et al., 2006; Ikeyama et al., 2008), etc.), and on spheromak-merging facilities such as the TS-3 (Ono et al., 1993) and MRX (Gerhardt et al., 2006). In addition, the stability of prolate and oblate FRCs has been analyzed by means of visible and x-ray photography with an end-on camera (Slough & Hoffman, 1993; Tuszewski et al., 1991), computer tomography reconstruction of the visible emission profile (Asai et al., 2006), as well as mode analysis of the external B_θ-magnetic probe array (Mirnov coil array) (Slough & Hoffman, 1993; Tuszewski et al., 1990, 1991; Kumashiro et al., 1993; Ikeyama et al., 2008) and the internal magnetic probe array (Ono et al., 1993; Gerhardt et al., 2006).

In the following sections, the formation methods for FRC plasma (Section 2) and the stability of FRC plasma (Section 3) are described based on these experimental results and some theoretical studies.

2. Formation methods for FRC plasma

An FRC is formed through a violent formation process dominated by self-organization. In this process, plasma pressure is built up, coinciding with the formation of reversed magnetic structure and plasma current drive within the diffusion time. The beta value of the FRC at the magnetic axis is infinite, and the volume-averaged beta value $<\beta>$ is nearly equal to one.

The plasma current density $j_\theta(r)$, the confinement magnetic field B_{ze}, the coil magnetic field B_{z0}, and the formed plasma pressure $p(r)$, satisfy the following condition:

$$I_\vartheta = \int_0^{r_s} j_\vartheta(r)dr \geq 2B_{z0}/\mu_0$$
$$\nabla p(r) = \frac{\partial p(r)}{\partial r} = j_\vartheta(r)B_z(r) \tag{1}$$

FRC plasma is traditionally formed by the field-reversed theta-pinch (FRTP) method (Armstrong et al., 1981). Since the 1990's, a variety of alternative formation methods have emerged (Ono, Y et al., 1993; Gerhardt et al. 2008; Slough & Miller, 2000; Knight & Jones, 1990; A. Hoffman et al., 2002; Guo et al., 2007; Logan et al., 1976; Davis, 1976; Greenly et al., 1986; Schamiloglu et. al., 1993). At the same time, the FRTP-based formation method has been significantly improved (Slough et al., 1989; Hoffman et al., 1993; Pietrzyk et al., 1987; Pierce et al., 1995; Guo et al., 2004, 2005; Asai et al., 2000; Binderbauer et al., 2010; Guo, et al., 2011). Recently initiated new formation methods include (1) counter-helicity spheromak-merging (CHSM) (Yamada et al., 1990; Ono et al., 1993; Gerhardt et al. 2008), (2) rotating magnetic field (RMF) (Slough & Miller, 2000; Knight & Jones, 1990; A. Hoffman et al., 2002; Guo et al., 2007), (3) field-reversed mirror configuration (FRM) driven by neutral beam injection (NBI) (Logan et al., 1976), relativistic electron beam (REB) (Davis, 1976), and intense light ion beam (ILIB) injections (Greenly et al., 1986; Schamiloglu et. al., 1993).

Improved FRTP methods have also introduced low inductive voltage and program formation by FRTP (Slough et al., 1989; Hoffman et al., 1993), the coaxial slow source (CSS) (Pietrzyk et al., 1987; Pierce et al., 1995), translation-trapping formation by FRTP (Guo et al., 2004, 2005; Asai et al., 2000), and collision FRC merging by FRTP (Binderbauer et al., 2010; Guo et al., 2011). Through these innovative new methods and improved FRTP methods, the

FRC lifetime has been prolonged to the order of several ms, and the confinement properties have also been improved [34]. The plasma parameters and lifetimes of FRCs formed by the above methods are summarized in Table 2.

Experimental and theoretical studies of FRC stability have mainly focused on elongated ($E > 1$) and oblate ($0 < E < 1$) FRC plasmas, formed by the FRTP (Slough & Hoffman, (1993), Fujimoto et al., 2002; Tuszewski, et al., 1990; Tuszewski et al., 1991; Kumashiro et al.,1993; Asai et al., 2006) and CHSW methods (Yamada et al., 1990; Ono et al., 1993; Gerhardt et al. 2008), respectively. Details of the two methods are introduced in the next section.

Formation method	B_e (T)	r_s (m)	n_p ($\times 10^{20}\, m^{-3}$)	T_i (keV)	Φ_p (mWb)	τ_{life} (ms)	E	$\bar{S}$
FRTP	0.3-2	0.05-0.24	5-500	0.1-15	0.4-12	0.03-0.4	2.5-10	0.5-5
FRTP+translation-trapping	0.01-0.06	0.12-0.5	0.4-5	0.2-0.5	1.5	0.2-0.4	5-8	0.8
FRTP+collision-merging	1.0-1.1	0.3-0.4	1	0.5-0.6	12	~1.0	5	1
RMF	0.006-0.025	0.03-0.45	0.007-0.17	0.02-0.2	1-10	1-2.5	1-3	-
Spheromak-merging	0.2-0.3	0.4-0.5	2	0.02-0.2	≤ 10	0.075-0.1	0.35-0.65	1-3
Spheromak-merging+CS	0.2-0.3	0.4-0.5	1	0.02-0.2	2-3	0.35-0.6	0.35-0.65	1-3

Table 2. FRC Plasma parameters for various formation methods

2.1 Field-reversed theta-pinch method (FRTP)

The schematic of a typical field-reversed theta-pinch device, NUCTE-III (Nihon University Compact Torus Experiment 3), is shown in Fig. 2 (Asai et al., 2006). A transparent fused silica glass discharge tube lies in a cylindrical one-turn coil. The tube is filled with a working gas (usually hydrogen or deuterium gas) by static filling or gas puffing, and then a z-discharge or inductive theta-discharge (θ-discharge) generates a pre-ionized plasma of the working gas, which is embedded in the reversed-bias field of 0.03-0.08 T, produced by 2 mF of the bias bank. A main bank of 67.5 μF rapidly reverses the magnetic field in the discharge tube (rising time of 4 μs). The circuit of the main bank is crowbarred on reaching the maximum current, and resistively decays with a decay time of 120 μs. A thin current sheet is initially formed around the inner wall of the discharge tube by an inductive electric field ($E_\theta = 0.5\, r dB_z/dt$), and shields the plasma from the rising forward field. The rising field works as a 'magnetic piston' to implode the plasma radially. At both ends of the coil, the reversed-bias field is reconnected with the forward field, and a closed magnetic structure is created. The tension formed due to the magnetic curvature produces a shock-like axial contraction. Then the radial and axial dynamics rapidly dissipate within about 20 μs, and the FRC plasma reaches an equilibrium/quiescent phase. Figure 3 shows the separatrix and the equi-magnetic surface

estimated by our improved excluded flux method, and the radial profile of bremsstrahlung (proportional to $n_e^2 / T_e^{0.5}$). An FRC plasma with a separatrix radius of 0.055 m and a length of 0.8 m is formed at about 20 μs, and is isolated from the discharge tube (r_t = 0.13 m).
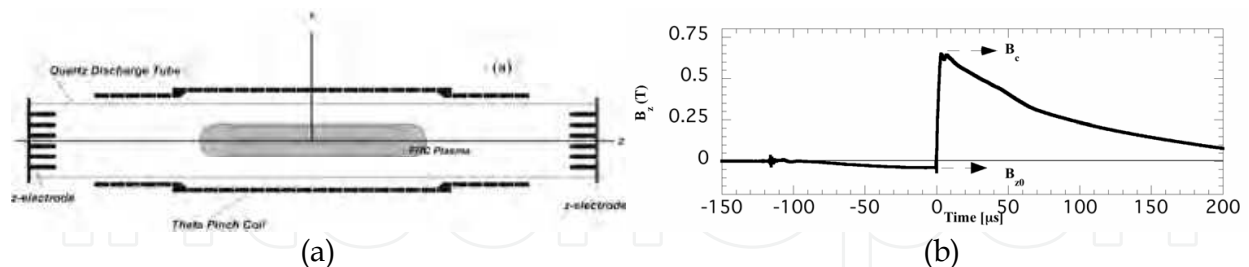

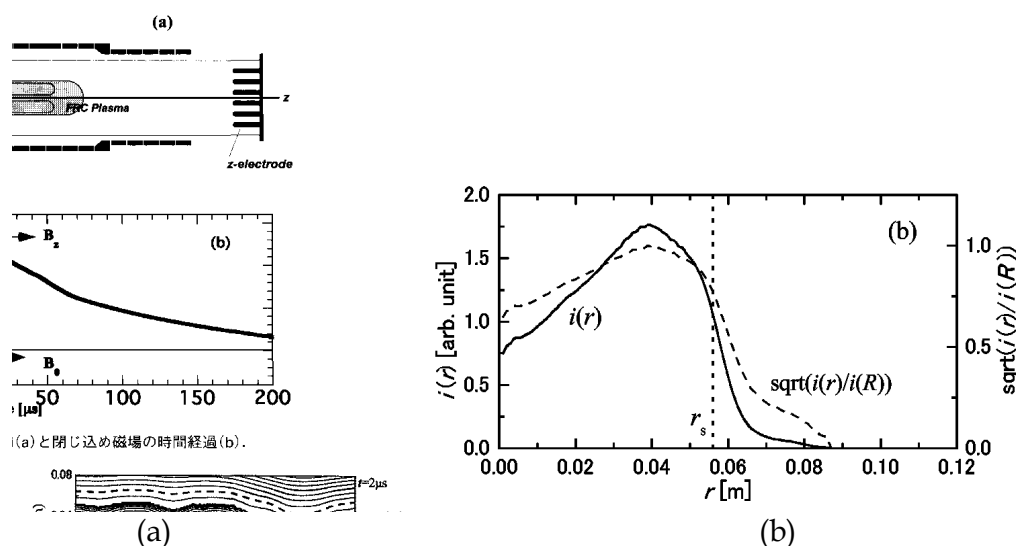Fig. 2. (a) Schematic diagram of NUCTE-III and (b) a typical waveform of magnetic field on FRTP method.method.

Fig. 3. (a) Time evolution of equi-magnetic surface of FRC at formation phase, and (b) pressure profile at equilibrium phase.

2.2 Counter-helicoty spheromak-merging method (CHSM)

A spheromak also belongs to the family of compact toroids. The plasma has a toroidal field nearly equal to the poloidal field. The spheromak is formed by various means, such as a simultaneous axial and θ discharge (z-θ discharge), a coaxial plasma gun, or a toroidal flux core containing both toroidal and poloidal winding (Ono et al., 1993; Gerhardt et al., 2006; Yamada et al., 1990; Ono et al., 1993; Gerhardt et al., 2008).

Two spheromaks, with a common geometric axis and opposite helicity (opposite toroidal fields) of equal value, are separately formed, and merge to form the FRC. If the respective helicity values of the spheromaks differ significantly, the merged plasma remains a spheromak (Ono et al., 1993; Yamada et al., 1990). This formation method naturally forms an oblate FRC, in contrast to the prolate FRC formed by the FRTP method.

In the Tokyo Spheromak 3 (TS-3) experiment, merging spheromaks are formed by z-θ discharge (Ono et al., 1993, 1997). The Swarthmore Spheromak Experiment (SSX) utilizes the coaxial plasma gun method (Cohen et al., 2003). The Tokyo Sheromak 4 (TS-4) and the Magnetic Reconnection Experiment (MRX) employ the flux core method (Gerhardt et al., 2006). The TS-3 device is illustrated in Fig. 4 (Ono et al., 1997). The time evolutions of the magnetic surface of the poloidal and toroidal fields, the toroidal flow, and the ion temperature, are also shown in the figure.
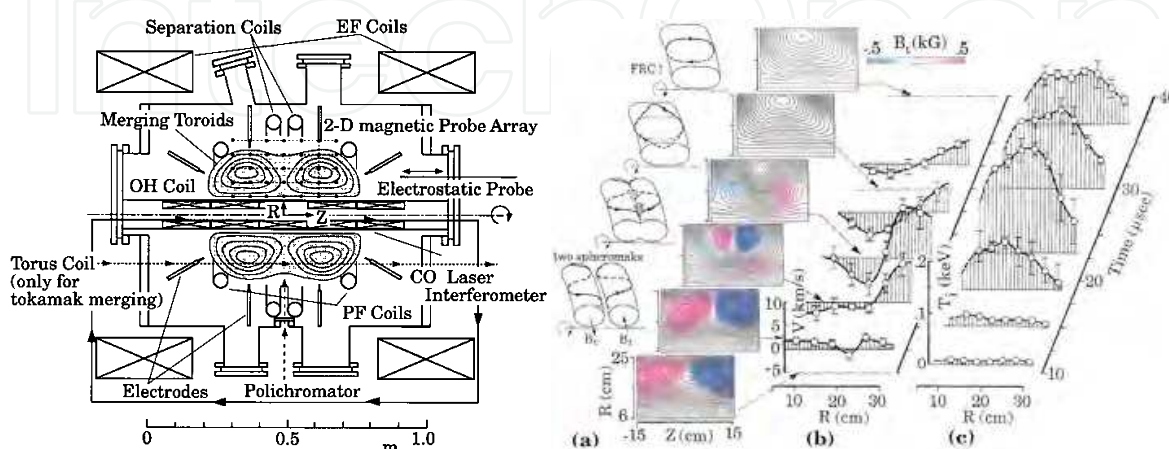
Fig. 4. (a) TS-3 merging device and 2D contours of poloidal flux surface and toroidal magnetic field on the R-Z plane; radial profiles of (b) ion toroidal velocity V, and (c) ion temperature (T_i), on the midplane, during the counter helicity merging of two spheromaks with equal but opposing B_t. The red and blue colors indicate the positive and negative amplitudes of B_t.

3. MHD behavior of FRCs

3.1 MHD behavior of prolate FRCs

3.1.1 General picture of prolate FRC MHD behavior

The global deformation of the internal structure of an FRC, and its time evolution, were investigated by means of an optical diagnostic system (Takahashi et al., 2004), combined with tomographic reconstruction, in the NUCTE facility (Asai et al., 2006). Fourier image transform was applied to the reconstructed image, and the correlation of global modes with $n = 1$ and 2 was investigated. The typical plasma parameters are separatrix radius of 0.06 m, separatrix length of 0.8 m, electron density of 2.5 x 10^{-20} m^{-3}, total temperature of 270 eV, particle confinement time of 80 μs, and $\bar{s}$ -value of 1.9. Figure 5 shows the time evolution of the 2D emissivity profile of bremsstrahlung of 550 nm. Here, the intensity of bremsstrahlung is proportional to $n_e^2/T_e^{0.5}$. Figure 5 (b) - (g) shows a reconstructed tomographic image of the cross-sectional structure at each phase indicated in the time history of line integrated electron density, measured along the y-axis (Fig. 5 (a)). Figure 5 (b) shows the emissivity structure 1 μs after application of the main compression field. We can see that the radial compression has started at the chamber wall. The following radial compression phase is shown in Fig. 5 (c). The circular boundary of the bright area indicates azimuthally uniform compression. After the formation phase, the equilibrium phase, with a circular cross-sectional structure, lasts approximately 20 μs (Fig. 5 (d)). The oscillation observed in the

latter phase is caused by rotational instability with toroidal mode number of n = 2. At the first stage of deformation, illustrated in Fig. 5 (e), the reconstructed cross section is deformed into an oval shape.
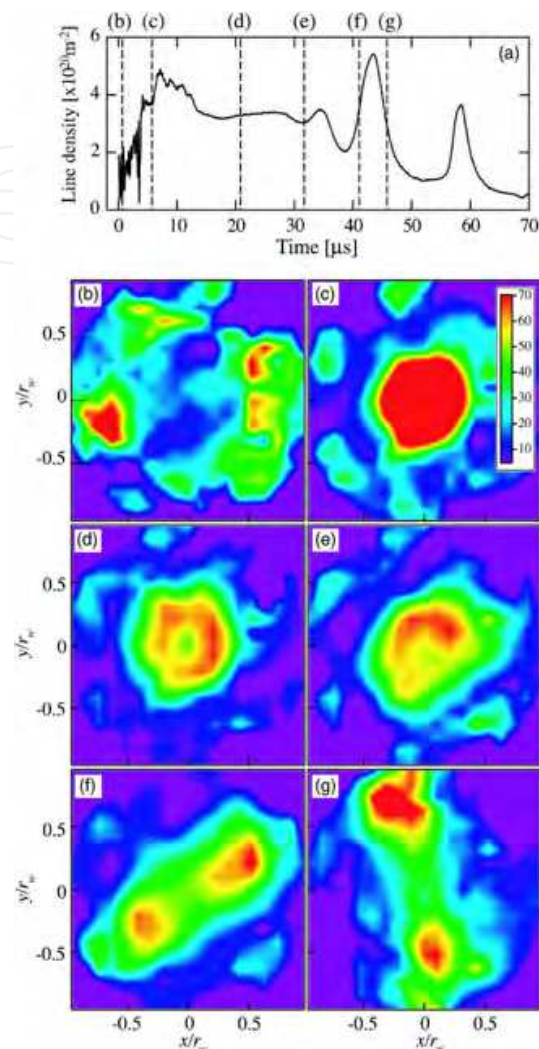

Fig. 5. (a) Time evolution of line integrated electron density, and (b) - (g) reconstructed cross-sectional structure of an FRC.

Generally, this deformation is called 'elliptical deformation.' However, the reconstructed image indicates an internal shift (n = 1) in an oval separatrix. In this rotational instability phase, deformation grows due to centrifugal distortion. In the early stage of the growth of instability, the structure of the FRC has a dumbbell-like shape, as shown in Fig. 5 (f). The internal structure at the final stage of the discharge is shown in Fig. 5 (g). The distribution of emissivity shows two clear peaks which orbit around the separatrix axis like binary stars. The analyzed time evolution of mode intensity and phase by the Fourier image transform are shown in Fig. 6. This result indicates that the n = 1 shift motion of the plasma column (wobble motion) increases prior to the growth of the n = 2 mode. The amplitude of n = 1 increases in the equilibrium phase of 20 – 30 μs. It is thus apparent that the dominant mode changes to n = 2 after a modest peak of n = 1. In the tomographic image of this transition region of n = 1 to 2 (Fig. 5 (e)), an internal shift of the bright area, which has a different

rotational phase from that of the oval plasma boundary, is seen. More specifically, this $n = 1$ shift motion and the rotational torque are possible sources of the $n = 2$ mode deformation. This result suggests that the suppression of this shift motion in the formation and equilibrium phase might impede the growth of $n = 2$ mode deformation.
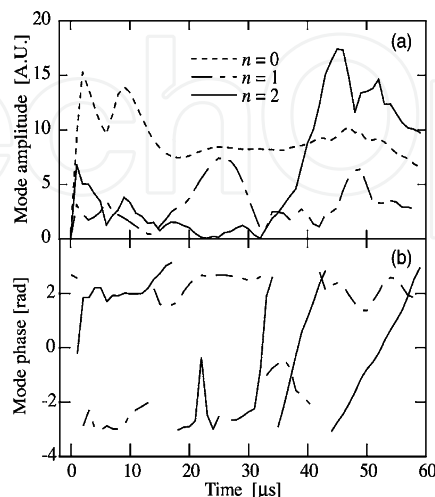

Fig. 6. Time evolution of (a) toroidal mode intensity, and (b) phase.

3.1.2 Stability of prolate FRCs with respect to rotational mode

These two global ideal modes driven by rotation—the $n = 1$ wobble and the $n = 2$ rotational instability—have been regularly observed in experiments. These rotational modes have been controlled by applying a straight or helical multipole field (Ohi et al., 1983; Shimamura & Nogi, 1986). The stability criterion (B_{sc} ($n = 2$)) of the straight multipole field of an m-pole for the $n = 2$ rotational instability has already been developed, on the basis of MHD equations, by Ishimura (Ishimura, 1984) as

$$B_{sc}(n = 2) = \frac{1}{2}\sqrt{\frac{\mu_0 \rho}{m-1}} r_s |\Omega| , \qquad (2)$$

where Ω, r, and μ_0 are, respectively, the rotational angular velocity of the $n = 2$ deformation (which is twice that of the angular velocity of the plasma column), the mass density of the plasma column, and the magnetic permeability of free space. On the other hand, the stability criterion for the $n = 1$ wobble motion (B_{sc} ($n = 1$)) has been derived from the experimental results of NUCTE-III (Fujimoto et al., 2002) as

$$B_{sc}(n = 1) = \frac{1}{f}\sqrt{\frac{\mu_0 \rho}{2(m-1)}} r_s \omega_{n=1} , \qquad (3)$$

where $\omega_{n=1}$ is the angular velocity of the $n = 1$ wobble motion, and f is an amplitude reduction coefficient which is defined by experiments with different pole numbers and is about 0.3 for the NUCTE FRCs. The ratio of B_{sc} ($n = 1$)/B_{sc} ($n = 2$) suggests that the amplitude of $n = 1$ mode motion can always be maintained at a low level by the application of B_{sc} ($n = 2$), provided $\omega_{n=1}/f < \omega_{n=2}$.

The experimental results of the FIX (FRC injection experiment) with neutral beam injection into FRC plasma formed by FRTP, indicate that the global $n = 1$ mode motion was controlled by neutral beam injection (Asai, et al., 2003). The neutral beam was injected obliquely to the axial direction due to the limited poloidal flux. The stabilization effects of ion rings confined by mirror fields at each end have been noted. Improved confinement properties (e.g., prolonged decay time of plasma volume and increased electron temperature) have also been observed.

TCS (Translation, Confinement and Sustainment) experiments at Washington University indicate that the $n = 2$ mode rotational instability can be controlled by the self-generated toroidal field, which converts from a toroidal into a poloidal field during the capture process of translated FRCs (Guo et al., 2004, 2005). The stabilization effect of the toroidal fields was investigated using the modified energy principle with the magnetic shear effect (Milroy et al., 2008). The following analytic stability criterion was derived as

$$B_{SC} > 0.66\sqrt{\mu_0 \rho} r_s \Omega \ . \tag{4}$$

This stability criterion is very similar to the one for the multipole field. This formula indicates that a relatively modest toroidal field, which is about 12% in comparison to the external poloidal field, can stabilize the FRC in the case of TCS experiments.

To supply the modest toroidal field to the FRC plasma, a magnetized coaxial plasma gun (MCPG) has been employed in the NUCTE facility (Asai et al., 2010). The MCPG generates a spheromak-like plasmoid which can then travel axially to merge with a pre-existing FRC. Since the MCPG is mounted on-axis and generates a significant helicity, it provides the FRC-relevant version of coaxial helicity injection (CHI) that has been applied to both spheromaks and spherical tokamaks. When CHI is applied, the onset of elliptical deformation of the FRC cross section is delayed until 45 - 50 μs from FRC formation, compared to an onset time of 25 μs without CHI. Besides delaying instability, MCPG application reduces the toroidal rotation frequency from 67 kHz to 41 kHz. Moreover, the flux decay time is extended from 57 to 67 μs. These changes occur despite the quite modest flux content of the plasmoid: ~ 0.05 mWb of poloidal and 0.01 mWb of toroidal flux, compared with the 0.4 mWb of poloidal flux in the pre-formed FRC. The MCPG introduces a different stabilization mechanism, which may be the same as that observed in translated FRCs, because of the existence of modest toroidal flux. The observed global stabilization and confinement improvements suggest that the MCPG can actively control the rotational instability.

In STX experiments, stabilization effects due to RMF have been observed. The stabilization effects can be attributed to two-fluid effects produced by rotational and ponderomotive forces. In TCS experiments, the stabilization effects of RMF on the $n = 2$ interchange mode and rotational mode have been reported (Guo et al., 2005). The stability criterion of RMF field strength (B_ω) was derived as

$$B_\omega \geq 1.14\sqrt{\rho \mu_0} r_s \Omega \ . \tag{5}$$

The stability diagram for FRC formed and sustained by the RMF at a different frequency is indicated in Fig. 6 of reference of Guo et al., 2005.

3.1.3 Stability of prolate FRCs with respect to tilt mode

In the FRX-C/LSM, which is a conventional FRTP device using non-tearing reconnection, the stability of FRC plasmas with $1 < \bar{s} < 3.5$ and $3 < E < 9$ (highly kinetic and elongated) was investigated using a Mirnov loop array of 64 external B_θ pick-up loops and a soft X-ray end-on camera (Tuszewski et al., 1991). Tilt-like asymmetries (the $n = 1$ axial odd component of B_θ) were found, which strongly correlates with FRC confinement. Tilt and other instabilities also appeared with an increase in the bias magnetic field and/or filling pressure (i.e., higher $\bar{s}$ - value). An increase in the bias field and filling pressure also coincidently causes strong axial dynamics, which triggers confinement degradation. These experimental results suggest that the tilt-stability condition for kinetic and elongated FRCs is in the range of $s/e < 0.2 - 0.3$ ($S^*/E < 3$) (Fig. 7), and becomes $s/e \sim 1$ for MHD-like FRC (Fig. 8). Strong axial dynamics during FRC formation results in lesser elongation of the FRC. Therefore it eventually fosters the growth of tilt instability. For an FRC with $s/e \sim 1$, the tilt instability grows from small initial perturbations, and becomes large enough to cause major plasma disruptions after 10 - 20 μs, which is 3 – 4 times longer than the growth time of instability. In the case of low filling pressures, higher order ($n = 2$ and 3) axially odd asymmetries are also observed. However, the amplitude of these modes is much less than that of the $n = 1$ tilt components. In the case of higher filling pressures, higher order modes appear earlier and grow vigorously.

In the LSX, using an improved FRTP formation method with a programmed formation scheme, the correlation between plasma distortions and the confinement properties was investigated (Slough & Hoffman, 1993). A B_θ probe array and an end-on soft X-ray camera were employed to determine separatrix movement, which might indicate the existence of lower order modes, such as tilt mode. Experiments were conducted over a large range of $\bar{s}$ ($1 < \bar{s} < 8$) and no correlation was observed between the quality of confinement and the B_θ signal. In fact, the confinement quality correlates more with the shape of the equilibrium radial profile than with $\bar{s}$. Details of the experimental results are summarized in Table 3.
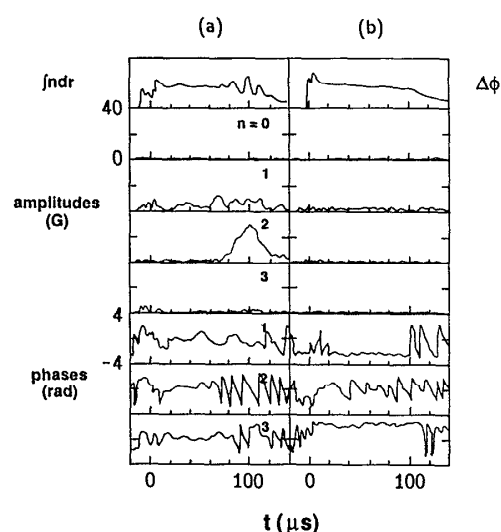

Fig. 7. Toroidal Fourier analysis of the B_θ for good confinement. The Fourier amplitudes and phases are shown as functions of time for (a) even and (b) odd components. The top trace of (a) is a line-integrated electron density and (b) diamagnetism.
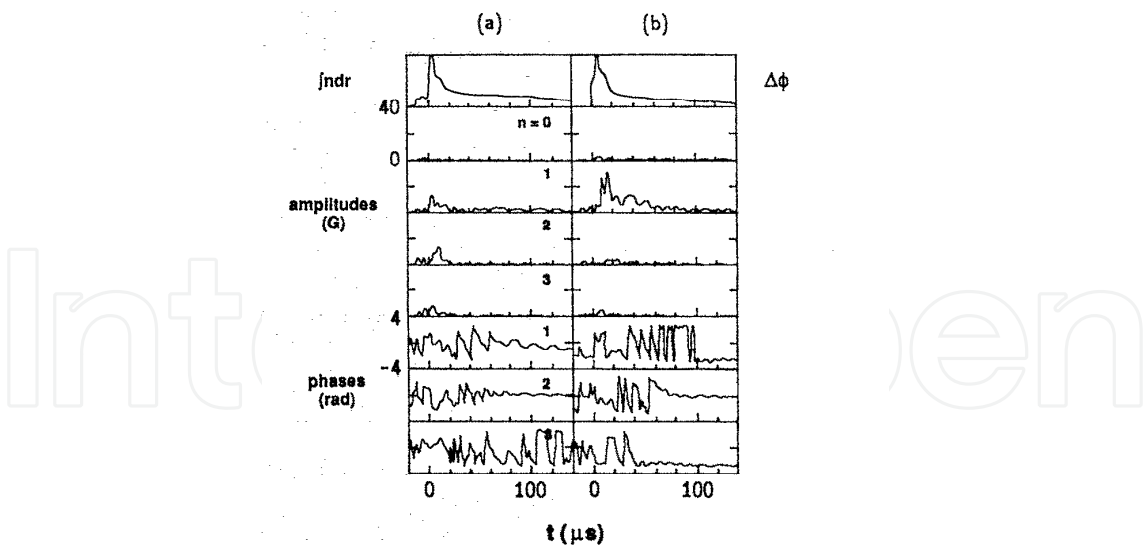
Fig. 8. Toroidal Fourier analysis of the B_θ for bad confinement. The Fourier amplitudes and phases are shown as functions of time for (a) even and (b) odd components The top trace of (a) is a line-integrated electron density and (b) diamagnetism.

Mode (*1)	Observed	Time	Confinement (degraded)	Loss of equilibrium
Co-interchange:				
N=1, M=1 (Tilt)	seldom	various	No	No
Interchange:				
N=1, M=0	occasional	equilibrium	No	No
N=1, M=0 (shift)	occasional	equilibrium	No	No
N=1, M=0 (wobble)	occasional	form/equilibrium	No	No
N>1, M=0 (flute)	seldom	formation	No	No
Rotation :				
N=2, M=1	always	late equilibrium	No (a)	Yes
N>2, M=1	seldom	late equilibrium	No (a)	Yes
Mode (*2)	**0bserved**	**Time**	**Confinement (degraded)**	**Loss of equilibrium**
Co-interchange:				
N=1, M=1 (Tilt)	seldom	various	No	No
Interchange:				
N=1, M=0 (sausage)	often	equilibrium	No	No
N=1, M=0 (shift)	occasional	equilibrium	No	No
N=1, M=0 (wobble)	occasional	form/equilibrium	No	No
N>1, M=0 (flute)	often	formation	No (b)	No
Rotation :				
N=2, M=1	always	late equilibrium	Yes	Yes
N>2, M=1	often	late equilibrium	Yes	Yes
Mode (*3)	**0bserved**	**Time**	**Confinement (degraded)**	**Loss of equilibrium**
Co-interchange:				
N=1, M=1 (Tilt)	seldom	various	No	No
Interchange:				
N=1, M=0 (sausage)	often	equilibrium	No	No
N=1, M=0 (shift)	occasional	equilibrium	No	No
N=1, M=0 (wobble)	occasional	form/equilibrium	No	No
N>1, M=0 (flute)	always	formation	Yes (c)	No (d)
Rotation :				
N=2, M=1	always	late equilibrium	Yes	Yes
N>2, M=1	often	late equilibrium	Yes	Yes

(*1) $1 \le \overline{s} \le 3$, (*2) $3 \le \overline{s} \le 5$, (*3) $5 \le \overline{s} \le 8$, (a) Confinement was not influenced until the mode amplitude was quite large, (b) Poor confinement correlated with non-optimal formation modes that resulted in large-amplitude flutes, (c) All very high-s discharges employed a non-optimal formation sequence, (d) A highly nonlinear flute destroyed the configuration formation

Table 3. Stability properties of FRC in LSX

3.1.4 Recent progress in theoretical understanding

To resolve this discrepancy between MHD predictions and experimental observation, significant progress in the theoretical understanding of FRC stability has been achieved. A host of stabilization effects—for example, the ion FLR effect, the effects of the Hall term and sheared ion flow, resonant particle effects, modern relaxation theory, and two-fluid flowing equilibrium—have been considered in the theoretical studies. Systematic studies of the stability properties of prolate and oblate FRC plasmas have also been presented in a series of Belova's works (Belova et al., 2000, 2001, 2003, 2004, 2006a, 2006b).
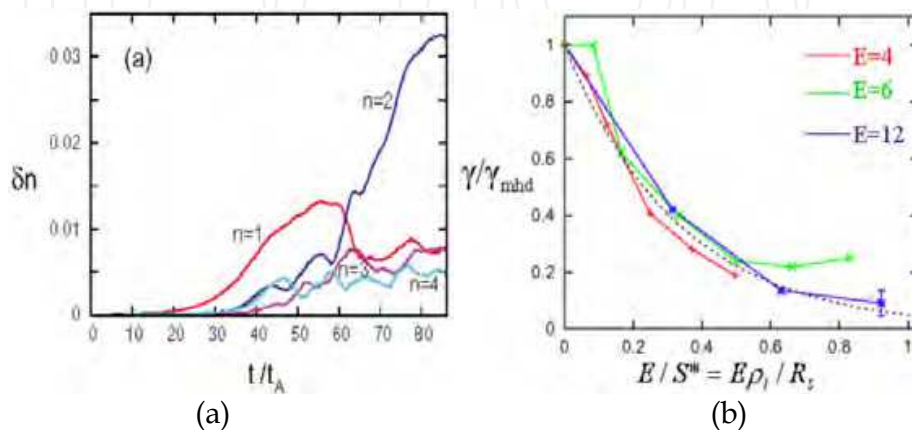
Fig. 9. (a) Time evolution of the amplitudes of different n-modes in prolate FRC with S*=20 and (b) Growth rate of n = 1 tilt instability for three elliptical FRC equilibria with E = 4, 6 and 12

The time evolution of the amplitudes (δn) of different n-modes in prolate FRC with S^* = 20 is shown in Fig. 9 (a) (Belova et al., 2004). Nonlinear saturation of the tilt modes, and growth of the n = 2 rotational mode due to ion toroidal spin-up, have been demonstrated. For oblate FRCs, the scaling of the linear growth rate of n = 1 internal tilt instability, with the parameter of S^*/E for elliptical FRC equilibria (E = 4, 6, 12), has also been investigated, and is shown in Fig. 9 (b) (Belova et al., 2006a). The growth rate of the n = 1 tilt mode is decreased in the range of S*/E < 3 ~ 4. For oblate FRC plasma, the stabilized region has been found for all n = 1 modes (the tilt mode, the radial shift, the interchange mode, and the co-interchange mode), with a closed conducting shell and neutral beam injection (Belova et al. 2006a, 2006b).
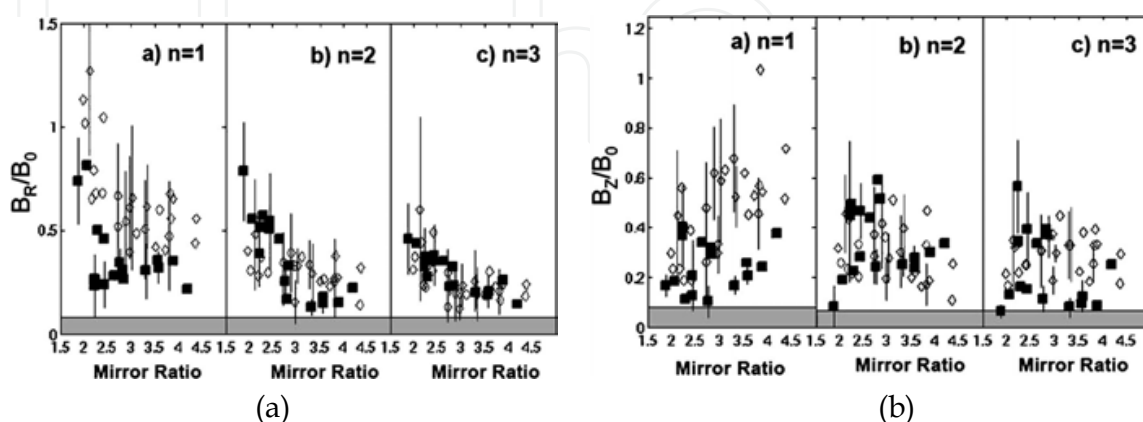

Fig. 10. Magnitude of (a) n = 1, (b) n = 2, (c) n = 3 perturbation in (a) B_r and (b) B_z. Hollow symbols are for cases without the center column, and solid symbols for cases with the center column.

3.2 MHD behavior and stability of oblate FRCs

In the MRX device, the stability of oblate FRC plasma was investigated. The plasma parameters are electron density of 0.5 - 2 x 10^{20} m^{-3}, ion temperature of ~18 eV, B_z of 300 - 200 G, E of 0.65 - 0.35, $\overline{s}$ of 1-3, and $\overline{s}/E$ of 2-5 (Gerhardt et al., 2006). Without a passive stabilizer (a hollow conducting center conductor), tilt and shift instability (n = 1 mode of Fig. 10 (a) and (b)) often appeared. The tilt mode limits the plasma lifetime. The tilt instability can be mitigated by either including a passive stabilizing conductor or forming highly oblate plasmas with a strong mirror field. Without the center column, the growth of the shift mode is reduced, apparently by the large magnetic fields on the outboard side of device. Large perturbations (n = 2 and 3) may still remain after passive stabilization is applied ((b) and (c) of Fig. 10 (a)). These perturbations have the characteristics of co-interchange modes, which have never been observed in conventional oblate FRCs. Such modes cause the early termination of the oblate FRC shape. These co-interchange modes can be stabilized in oblate plasma with a high mirror ratio, and this produces an FRC with maximum configuration lifetime.

4. Summary

In Table 4, the MHD stability properties of both prolate and oblate FRCs are summarized (Yamada et al., 2007). In oblate FRC plasma, the global mode (n = 1 external tilt and shift mode, co-interchange mode) is unstable. But these modes can be stabilized by employing a close-fitting conducting shell or shaping with a strong external magnetic field. In prolate plasma, the internal tilt mode and co-interchange mode are MHD-unstable. However, these can be stabilized by nonlinear effects, such as FLR, rotation and sheared flow. It is difficult to observe these modes clearly in the experiments. The most destructive rotational mode (n = 2), and wobble (n = 1) mode, are almost always observable in experiments. Active stabilization methods without degradation of confinement, such as CHI, need to be developed.

	Prolate [E>1]	Oblate [E<1]
Internal Tilt, n=1	MHD unstable, stabilized by FLR, rotation and nonlinear effects for S*<20, E $\geq$ 5.	MHD Stable
External Tilt and Radial Shift, n=1	MHD stable	MHD unstable, stabilized by conducting shell
Co-interchange, n>1	MHD unstable, stabilized by FLR	MHD unstable, stabilized by NBI + conducting shell
Interchange, n>1	MHD unstable, stabilized by compressional effects	MHD unstable, stabilized by compressional effects
Rotational, n=2	MHD unstable, stabilized by quadrupole field, RMF and conducting shell	MHD unstable, stabilized by quadrupole field, RMF and conducting shell

Table 4. Stability properties of prolate and oblate FRCs

5. References

Armstrong, W. T., et al., (1981), Field-reversed experiments (FRX) on compact toroids, *Physics of Fluids* Vol. 24, No.11, pp. 2068-2088

Asai, T., et al., (2000), Experimental evidence of improved confinement in a high-beta field-reversed configuration plasma by neutral beam injection, *Phys. Plasmas*, Vol. 7, No.6, pp. 2294-2297

Asai, T., et al., (2003), Stabilization of global movement on a field-reversed configuration due to fast neutral beam ions, *Physics of Plasmas*, Vol.10, No.9, pp. 3608-3613

Asai, T., et al., (2006), Tomographic reconstruction of deformed internal structure of a field-reversed configuration, *Physics of Plasmas* Vol. 13, 072508, pp. 1-6.

Asai, T., et al., (2010), Active Stability Control of a High-Beta Self-Organized Compact Torus, *23rd IAEA Fusion Energy*,ICC/P5/01, Available from http:// www-pub.iaea.org/mtcd/meetings/cn180_papers.asp

Belova, E. V., et al., (2000), Numerical study of tilt stability of prolate field-reversed configurations, *Physics of Plasmas*, Vol.7, No. 12, pp. 4996-5006

Belova, E. V., et al., (2001), Numerical study of global stability of oblate field-reversed configurations, *Physics of Plasmas*, Vol.8, No.4, pp. 1267-1277

Belova, E. V., et al., (2003), Kinetic effects on the stability properties of field-reversed configurations. I. Linear stability, *Physics of Plasmas*, Vol.10, No.11, pp. 2361-2371

Belova, E. V., et al., (2004), Kinetic effects on the stability properties of field-reversed configurations. II. Nonlinear évolution, *Physics of Plasmas*, Vol.11, pp. 2523-2531

Belova, E. V., et al., (2006), Advances in the numerical modeling of field-reversed configurations, *Physics of Plasmas,* Vol. 13, 056115, pp. 1-5

Belova, E. V., et al., (2006), Numerical study of the formation, ion spin-up and nonlinear stability properties of field-reversed configurations, *Nuclear Fusion,* Vol.46, pp. 162-170

Binderbauer, M. W., et al., (2010), Dynamic Formation of a Hot Field Reversed Configuration with Improved Confinement by Supersonic Merging of Two Colliding High-Compact Toroids, *Physical Review Letters,* Vol. 105, 045003, pp.1-4.

Cohen, C. D., et al., (2003), Spheromak merging and field reversed configuration formation at the Swarthmore Spheromak Experiment, *Physics of Plasmas*, Vol. 10, No.5 pp. 1748-1754

Davis, H. A., et al., (1976), Generation of Field-Reversing E Layers with Millisecond Lifetimes, *Physical Review Letters,* Vol.37, No.9, pp. 542-545

Freidberg, J. P. and Pearlstein, L. D., (1978), Rotational instabilities in a theta pinch, *Physics of Fluids,* Vol. 21, 1207-1217

Fujimoto, K., et al., (2002), Control of a global motion on field-reversed configuration, *Physics of Plasmas* Vol.9, No.1, pp. 171-176

Gerhardt, S. P. et al., (2006), Equilibrium and stability studies of oblate field-reversed configurations in the Magnetic Reconnection Experiment, *Physics of Plasmas* Vol. 13, 112508, pp.1-18

Gerhardt, S. P., et al., (2008), Field-reversed configuration formation scheme utilizing a spheromak and solenoid induction, *Physics of Plasmas*, Vol.15, 022503, pp.1-11

Greenly, J. B., et al., (1986), Efficient proton ring trapping in an ion ring experiment, *Physics of Fluids*, Vol. 29, No.4, pp.908-911

Guo, H. Y., et al., (2004), Flux Conversion and Evidence of Relaxation in a High- Plasma Formed by High-Speed Injection into a Mirror Confinement Structure, *Physical Review Letters*, Vol. 92, 245001, pp. 1-4

Guo, H. Y., et al., (2005), Observations of Improved Stability and Confinement in a High-β Self-Organized Spherical-Torus-Like Field-Reversed Configuration, *Physical Review Letters*. Vol. 94, 175001, pp. 1-4

Guo, H. Y., et al., (2005), Stabilization of Interchange Modes by Rotating Magnetic Fields, *Physical Review Letters* , Vol.94, 185001, pp. 1-4

Guo, H. Y., et al., (2007), Improved confinement and current drive of high temperature field reversed configurations in the new translation, confinement, and sustainment upgrade device, *Physics of Plasmas,* Vol.14, 112502, pp.1-7

Guo, H. Y., et al., (2011), Formation of a long-lived hot field reversed configuration by dynamically merging two colliding high- compact toroids, *Physics of Plasmas*, Vol. 18, 056110, pp. 1-10

Hoffman, A., et al., (1993), Field reversed configuration lifetime scaling based on measurements from the Large s Experiment, *Nuclear Fusion*, Vol.33, No.1, pp.27-38

Hoffman, A., et al., (2002), Formation and steady-state maintenance of field reversed configuration using rotating magnetic field current drive, *Physics of Plasmas*, Vol.9, No.1, pp. 185-200,

Ikeyama, T., et. al., (2008), Analysis of magnetic probe signals including effect of cylindrical conducting wall for field-reversed configuration experiment, *Review of Science Instruments* Vol.79, 063501, pp. 1-10.

Ishimura, T., (1984), Multipole-field stabilization of the rotational instability in a theta pinch. I, *Physics of Fluids,* Vol. 27, No.8, pp. 2139-2150

Knight, A. J. & Jones, I. R., (1990), A quantitative investigation of rotating magnetic field current drive in a field-reversed configuration, *Plasma Physics and Controlled Nuclear Fusion*, Vol. 32, No. 8, pp. 575-605

Kumashiro, S., et al., (1993), Sources of Fluctuating Field on Field-Reversed Configuration Plasma, *Journal of the Physical Society of Japan*, Vol.62, No.5, pp. 1539-1551

Logan, G. B., et al., (1976), High-β , Gas-Stabilized, Mirror-Confined Plasma, *Physical Review. Letters*, Vol. 37, No.22, pp. 1468-1471

Milroy, R. D., et al., (2008), Toroidal field stabilization of the rotational instability in field-reversed configurations, *Physics of Plasmas* Vol.15, 022508, pp. 1-8

Momota, H., et al., (1992), CONCEPTIONAL DESIGN OF THE D-3He REACTOR ARTEMIS, Fusion Technology Vol. 21, pp.2307-2323

Ohi, S., et al., (1983), Quadrupole stabilization of the n=2 rotational instability of a field-reversed theta-pinch plasma, *Physical Review Letters,* Vol.51, No.12, pp.1042-1045

Ono, Y., et al., (1993), Experimental investigation of three-dimensional magnetic reconnection by use of two colliding spheromaks, *Physics of Fluids B*, Vol.5, No. 10, pp. 3691-3701,

Ono, Y., et al., (1997), Experimental investigation of three-component magnetic reconnection by use of merging spheromaks and tokamaks, *Physics of Plasmas,* Vol. 4, No.5, pp. 1953-1963.

Pierce, W. F., et al., (1995), Stabilization and saturation of the ideal tilt mode in a driven annular field-reversed configuration, *Physics of Plasmas*, Vol. 2, No.3, pp. 846-858

Pietrzyk, Z. P., et al., (1987), Initial results from the Coaxial Slow Source FRC device, *Nuclear. Fusion*, Vol. 27, No.9, pp. 1478-1487

Schamiloglu, E., et. al., (1993), Ion ring propagation in a magnetized plasma, *Physics of Fluids B*, Vol.5, No8, pp. 3069-3078

Shimamura, S. & Nogi, Y. , (1986), Helical Quadrupole Field Stabilization of Field Reversed Configuration Plasma, *Fusion Technology*, Vol.9, No.1, pp. 69-74

Slough, J. T., et al., (1989), Formation studies of field-reversed configurations in a slow field-reversed theta pinch, *Physics of Fluids B,* Vol.1, No.4, pp. 840-850

Slough, J. T. & Hoffman, A. L., (1993), Stability of field-reversed configurations in the large s experiment (LSX), *Physics of Fluids B*, Vol.5, No.12, pp. 4366-4377

Slough, J. T., & Miller, K., (2000), Flux generation and sustainment of a field reversed configuration with rotating magnetic field current drive, *Physics of Plasmas.* Vol.7, No.5, pp.1945-1950

Slough,J. T., et al., (2007), Compression, Heating and Fusion of Colliding Plasmoids by a Z-theta Driven Plasma Linear, *Journal of Fusion Energy*, Vol. 26, No. 1-2, pp. 191-197

Slough, J. T., et al., (2007), The Pulsed High Density Experiment: Concept, Design, and Initial Results, *Journal of Fusion Energy,* Vol. 26, Numbers 1-2, pp. 199-205

Steinhauer, L. C., (2011), Review of field-reversed configurations , *Physics of Plasmas, Vol.* 18, 070501, pp. 1-38

Seyler, C. E., (1979), Vlasov–fluid stability of a rigidly rotating theta pinch, *Physics of Fluids Vol.* 22, pp. 2324-2330

Taccetti, J. M., et al., (2003), FRX-L: A field-reversed configuration plasma injector for magnetized target fusion, *Review of Science Instruments, Vol 74, No.10,* pp.4314-4323

Takahashi, T., et al., (2004), Multichannel optical diagnostic system for field-reversed configuration plasmas, *Review of Science. Instruments*, Vol. 75, No.12, pp. 5205-5212.

Tuszewski, M., (1988), Field reversed configurations, *Nuclear Fusion,* Vol. 28, No.11, pp. 2033-2092

Tuszewski, M., et al., (1990), The n=1 rotational instability in field-reversed configurations, *Physics of Fluids B Vol. 2*, No.11 pp. 2541-2543

Tuszewski, M., et al., (1991), Axial dynamics in field-reversed theta pinches II, Stability, *Physics of Fluids B* Vol.3, No.3, pp. 2856-2870

Yamada, M., et al., (1990), Magnetic reconnection of plasma toroids with cohelicity and counterhelicity, *Physical. Review Letters*, Vol. 65, No.6, pp. 721-724

Yamada, M., et al., (2007), A Self-Organized Plasma with Induction, Reconnection, and Injection Techniques: the SPIRT Concept for Field Reversed Configuration Research, *Plasma and Fusion Research*, Vol. 2, 004, pp. 1-14
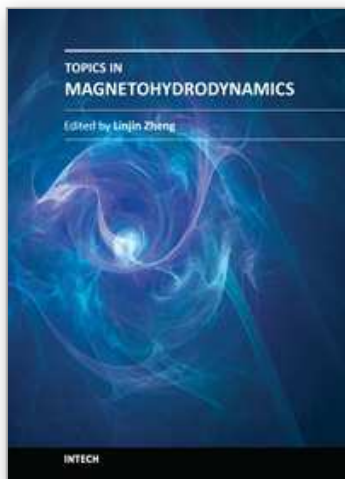
Topics in Magnetohydrodynamics

Edited by Dr. Linjin Zheng

To understand plasma physics intuitively one need to master the MHD behaviors. As sciences advance, gap between published textbooks and cutting-edge researches gradually develops. Connection from textbook knowledge to up-to-dated research results can often be tough. Review articles can help. This book contains eight topical review papers on MHD. For magnetically confined fusion one can find toroidal MHD theory for tokamaks, magnetic relaxation process in spheromaks, and the formation and stability of field-reversed configuration. In space plasma physics one can get solar spicules and X-ray jets physics, as well as general sub-fluid theory. For numerical methods one can find the implicit numerical methods for resistive MHD and the boundary control formalism. For low temperature plasma physics one can read theory for Newtonian and non-Newtonian fluids etc.

How to reference

In order to correctly reference this scholarly work, feel free to copy and paste the following:

INTECH
open science | open minds